



# Nanostructure and damage characterisation of bitumen under a low cycle strain-controlled fatigue load based on molecular simulations and rheological measurements

Yangming Gao<sup>a</sup>, Xueyan Liu<sup>b</sup>, Shisong Ren<sup>b</sup>, Eli I. Assaf<sup>b</sup>, Pengfei Liu<sup>c,\*</sup>, Yuqing Zhang<sup>d</sup>

<sup>a</sup> Built Environment and Sustainable Technologies (BEST) Research Institute, Liverpool John Moores University, L3 3AF, Liverpool, United Kingdom

<sup>b</sup> Section of Pavement Engineering, Faculty of Civil Engineering & Geosciences, Delft University of Technology, 2628 CN, Delft, the Netherlands

<sup>c</sup> Institute of Highway Engineering, RWTH Aachen University, 52074, Aachen, Germany

<sup>d</sup> School of Transportation, Southeast University, 211189, Nanjing, China

## ARTICLE INFO

Handling Editor: Dr Uday Vaidya

### Keywords:

Bitumen  
Fatigue damage  
Nanostructure  
MD simulation  
Rheometer measurement

## ABSTRACT

Bitumen fatigue resistance is critical to determine the overall fatigue performance and service life of asphalt pavements. However, the mechanisms responsible for fatigue damage of bitumen have previously not been well understood. Molecular dynamics (MD) simulation has recently emerged as a powerful computer-aided numerical technique to model the microscopic failure behaviours in materials. This study aims to use the MD method to investigate the molecular origin of bitumen fatigue damage. The molecular models of the virgin and aged PEN70/100 bitumen were firstly constructed based on their saturate, aromatic, resin and asphaltene (SARA) four fractions. An MD equilibrium was run on the developed bitumen models with the assigned interatomic potentials. Following an MD-based tensile simulation, a strain-controlled fatigue simulation was performed to study the nanostructure and damage behaviours of the virgin and aged bitumen under fatigue loading by calculating the stress-strain response, potential energy, molecular structure and nanovoid volumes. Furthermore, a rheometer measurement was also conducted to characterise the fatigue damage of the bitumen directly by a crack length at the macroscale. Results indicate that the bitumen molecules become unfolded and tend to align along the loading direction when fatigue loading was applied. The change in the molecular configuration helped the molecular chains move closer together and thus contributed to the reduction of the intermolecular interactions including the van der Waals and Coulombic energies. With the increasing load cycles, nanovoids were formed and grew in the bitumen through molecular rearrangement and movement, leading to microscopic fatigue damage of the bitumen. It was found that the aged bitumen produced more severe fatigue damage than the virgin bitumen, which was indicated by the MD-based nanovoid volume at the molecular scale and the DSR-based crack length at the macroscale. The findings from MD simulation provide a fundamental understanding of the molecular origin of fatigue damage, that cannot be experimentally detected for bitumen materials.

## 1. Introduction

Bitumen produced from petroleum (crude oil) is a complex viscoelastic material. The bitumen commonly serves as a binder between mineral aggregates in asphalt mixtures used for the construction and maintenance of asphalt pavement. The inherent ability of the bitumen to resist fatigue damage is critical to ensure fatigue performance and service life of the asphalt mixture and pavement. Therefore, fatigue failure of the bitumen has long been a major concern in the field of road infrastructure and materials. Based on Dynamic Shear Rheometer (DSR)

measurements, research efforts have been made in the past few decades to characterise the fatigue performance of the bitumen [1]. To evaluate the fatigue resistance of the bitumen, researchers have proposed several fatigue parameters such as the fatigue factor  $|G^*| \cdot \sin \delta$  used in the Superpave Performance Grading (PG) system, dissipated energy ratio (DER) [2–4], ratio of dissipated energy change (RDEC) [5–7] as well as fatigue law based on the viscoelastic continuum damage (VECD) theory [8–10]. Although these parameters are being used for fatigue characterisation of the bitumen, the mechanisms leading to fatigue damage of the bitumen are still not well known.

\* Corresponding author.

E-mail address: [liu@isac.rwth-aachen.de](mailto:liu@isac.rwth-aachen.de) (P. Liu).

<https://doi.org/10.1016/j.compositesb.2024.111326>

Received 5 October 2023; Received in revised form 12 February 2024; Accepted 17 February 2024

Available online 19 February 2024

1359-8368/© 2024 The Authors. Published by Elsevier Ltd. This is an open access article under the CC BY-NC-ND license (<http://creativecommons.org/licenses/by-nc-nd/4.0/>).

To understand the underlying fatigue damage mechanisms, three key questions have to be answered, namely (a) what the damage in the bitumen looks like, (b) how the damage grows, and (c) when the damage is initiated. Researchers have found that the damage of bitumen under a DSR fatigue load is a circumferential crack that starts at the edge of the bitumen sample and propagates toward its centre [11,12]. Using viscoelastic damage mechanics, a DSR-based cracking (DSR-C) model was developed in the authors' previous study [13] to predict the fatigue crack length in the bitumen. In the DSR-C model, the crack length can be determined using the shear moduli and phase angles of the bitumen measured by the DSR. The crack length provides a more efficient parameter to directly evaluate the bitumen's resistance to fatigue damage. Following the crack length calculated by the DSR-C model, the fatigue crack propagation of the bitumen was modelled using pseudo J-integral Paris' law in a separate work [14] to describe how the damage grows. One of the important findings is that the model coefficients ( $A$  and  $n$ ) from the Paris' law are fundamental material properties, which are independent of loading frequency or strain amplitude. Furthermore, a fatigue crack initiation criterion of the bitumen was developed based on viscoelastic Griffith's fracture mechanics to determine when the damage is initiated [15]. It was found that there is edge flow damage at the initial stage (around the first 1000 cycles) of bitumen fatigue cracking. These works from the fundamental mechanical perspective have addressed the three key questions mentioned above at the macroscale. However, further studies at the microscale are still needed to elucidate the microscopic mechanisms of fatigue damage initiation.

Failure mechanisms of the bitumen at the microscale have been studied by several researchers. Harvey and Cebon [16] observed the failure process of a viscoelastic film in a tension test based on a photographic technique. It was revealed that voids first became visible and then began to nucleate at the fracture surface during testing. Poulikakos et al. [17,18] investigated the time evolution of failure phenomena of a micro-scale thin bitumen film under direct tension tests using video recording and image processing techniques. The results showed the failure stages during tensile mechanical loading included the formation of striations, void nucleation and growth, filamentation and large ductile flow before fracture. Sultana and Bhasin [19] studied the rheology and mechanical properties of the bitumen with different chemical compositions. It was found that the bitumen containing the higher percentage of polar fractions had smaller and more frequent cavities at the fracture surface. More recently, Hajj et al. [20] performed real-time microscopic and rheometric observations of cavitation instability underlying micro-crack formation in a thin and confined film of bitumen under a monotonic mechanical strain using dark field microscopy. The formation and rapid growth of small cavities were observed during testing. A three-stage model was proposed to characterise the nucleation of the first cavity, subsequent cavities and the growth of existing cavities. Based on such advanced photographic techniques, these studies successfully revealed the microscopic mechanisms of the bitumen failure under tensile loading. However, significant challenges remain in the experimental detection of initial microscopic damage (i.e., micro-crack or nanovoids) inside the bitumen under fatigue loading due to the limitations in the time and length scales.

With the recent development of high-performance computation, computer-aided numerical techniques have been widely applied for the microscopic modelling and simulations of bituminous materials [21–24]. One of the most important computer-aided techniques is molecular dynamics (MD) simulation [25,26]. The MD-based computational approach has become a powerful tool to investigate the failure behaviours of bitumen at the microscopic scale. Hou et al. [27,28] used MD simulation to investigate the micromechanical behaviours of bitumen under tensile loading. Du et al. [29] studied the deformation behaviours of bitumen under nanoindentation. Sun and Wang [30] simulated a tensile test to study the nano-crack formation in bitumen with different SARA fractions. It was reported that the bitumen with a higher density and more asphaltene exhibited greater resistance to crack

initiation. The MD simulation has also been employed to study the microscopic deformation and failure behaviours of bitumen with mineral aggregate in the pull-off test [31–35]. These studies demonstrate that the MD simulation can be used to fundamentally interpret the microscopic failure mechanisms of bitumen under external loading through direct observation of molecular behaviours inside the material. Therefore, it is desired to investigate the microscopic mechanisms of fatigue damage in bitumen using the MD simulation to overcome the difficulty of experimental observation.

The main objective of this study is to use an MD computational approach to investigate the nanostructure and damage behaviours of the bitumen under fatigue loading. The molecular models of the virgin and aged PEN70/100 bitumen were firstly constructed based on their experimental data in terms of their elements, functional groups, molecular weights, as well as their saturate, aromatic, resin and asphaltene (SARA) four fractions. The interatomic potentials in the molecular models were defined using a Condensed-phase Optimized Molecular Potentials for Atomistic Simulation Studies (COMPASS) force field. The molecular models were validated by comparing the predicted thermodynamic properties with the experimental and reference data. After an MD-based tensile simulation, a strain-controlled fatigue simulation was performed at the temperature of 20 °C. Based on the simulation results, the nanostructures and damage behaviours of the bitumen were studied by calculating the stress-strain response, potential energy, molecular structure and nanovoid volumes during fatigue loading. Furthermore, the effects of ageing on the microscopic fatigue damage of the bitumen were analysed using the proposed MD-based computational approach. Finally, the fatigue damage of the virgin and aged bitumen at the macroscale was also directly characterised by crack length based on the rheometer measurements. The present innovative research addresses the fatigue crack initiation problem of the bitumen at the microscale using a molecular dynamics (MD) method and provides a fundamental understanding of the molecular origin of bitumen fatigue damage, which has not been investigated in the past due to the challenges in the time and length scales. This research work is focused on the microscopic fatigue damage mechanism, which is completely different from the existing studies that mainly involved the characterisation of the macroscopic fatigue performance and the microscopic tensile failure.

## 2. Methodology

### 2.1. Materials

The bitumen used in this study is PEN70/100 bitumen from Total Nederland NV. Table 1 presents its physical properties and chemical composition. To investigate the ageing effect, the virgin bitumen was subjected to a long-term ageing process in the laboratory. Following a thin film oven test (TFOT) at 163 °C for 5 h, a pressure ageing vessel (PAV) test was conducted for 20 h at a temperature of 100 °C and a pressure of 2.1 MPa to prepare the aged bitumen.

**Table 1**  
Physical properties and chemical composition of PEN 70/100 bitumen.

Properties	Value	
Penetration @ 25 °C (1/10 mm)	91	
Softening point (°C)	48	
Dynamic viscosity @ 135 °C (Pa·s)	0.8	
Density @ 25 °C (g/cm <sup>3</sup> )	1.017	
Chemical fractions (wt %)	Saturate (S)	3.6
	Aromatic (A)	53.3
	Resin, (R)	30.3
	Asphaltene (A)	12.8
	Carbon (C)	84.06
Element composition (wt %)	Hydrogen (H)	10.91
	Oxygen (O)	0.62
	Sulphur (S)	3.52
	Nitrogen (N)	0.9

## 2.2. Molecular models for virgin and aged bitumen

Bitumen is a mixture of various hydrocarbons with a complex chemical composition. It can be divided into saturates (S), aromatics (A), resins (R) and asphaltenes (A) four fractions based on its physical properties and solubility. Li and Greenfield [36] have proposed 12 types of molecules to represent SARA fractions in the bitumen. In this study, the 12 types of molecules are adopted as the basis of molecular models for virgin and aged PEN70/100 bitumen.

Based on the FTIR results, it was found that the sulfoxide functional groups that were not taken into consideration in Greenfield's 12 types of molecules exist in the virgin PEN70/100 bitumen [37]. Thus, the sulfoxide functional groups are supplemented in the benzobisbenzothiophene and the thioisorenieratane which are the only two molecules containing sulphur atoms in the SARA fractions. Meanwhile, the other ten molecules of SARA fractions remain the same as those in Greenfield's 12 types of molecules. All the molecules of SARA fractions used for the virgin PEN70/100 bitumen in this study are shown in Fig. 1.

The molecules used for the aged PEN70/100 bitumen can be determined by introducing the oxygen atoms to the molecular structures of SARA fractions in the virgin bitumen based on the mechanism of bitumen oxidative ageing. The ketones formed at benzylic carbon atoms and sulfoxides formed at sulphur atoms were identified as the major oxidation products in the molecules during the bitumen ageing [38–40]. The authors' previous study [37] has proposed the oxidised molecules of SARA fractions with different ageing levels. Four oxidised molecules used for the aged PEN70/100 bitumen in this study are illustrated in Fig. 1, including oxidised PHPN, oxidised thioisorenieratane, oxidised benzobisbenzothiophene and oxidised asphaltene-thiophene.

Once the virgin and oxidised molecules of the SARA fractions are determined, the molecular models of the virgin and aged PEN70/100 bitumen can be constructed based on their SARA mass fractions measured by a thin-layer chromatography with flame ionization detection (TLC-FID) test. Table 2 presents the SARA fractions from the model and experiment for the virgin and aged PEN70/100 bitumen amples. The SARA fractions in the models agree well with the experimental

results for both the virgin and aged bitumen. It also should be noted that the amount of ketone and sulfoxide functional groups and the molecular weight values in the molecular models of the virgin and aged bitumen were verified by comparing with the experimental data obtained from the attenuated total reflectance-Fourier-transform infrared (ATR-FTIR) spectroscopy and gel permeation chromatography (GPC) tests in the authors' previous study [37].

## 2.3. Molecular dynamics (MD) equilibrium

### 2.3.1. MD method

Molecular dynamics (MD) method is a computer-aided numerical technique to simulate the atomistic movements and interactions in a classic many-body system based on Newton's law of motions and statistical mechanics. Typically, an MD simulation involves the following components [32]: (1) the potential function to determine the forces among the atoms, (2) the classical mechanics to calculate the acceleration and instantaneous velocity of atoms, (3) the integration algorithm to solve for the trajectory and subsequently update the potential among the atoms, and (4) the statistical mechanics to interpret the system properties. Fig. 2 shows a calculation procedure in MD simulation.

This MD method calculates the motions of  $N$  atoms in a system as a function of time. In classical statistical mechanics, the trajectories including positions and velocities are computed by integrating Newton's second law, as described in Eq. (1). The initial atomic velocities are assigned randomly by a Maxwell-Boltzmann distribution. Eq. (1) can be integrated by several robust algorithms that require finite differencing and a suitable time step [41]. The time step conserves the total Hamiltonian of the system.

$$m_i \frac{\partial^2 r_i}{\partial t^2} = - \frac{\partial U}{\partial r_i} \equiv F_i \quad (1)$$

where  $m_i$  is the mass of atom  $i$ ,  $r_i$  is the coordinate of atom  $i$ ,  $\partial U$  is the interatomic potential, and  $F_i$  is the internal force of atom  $i$ .

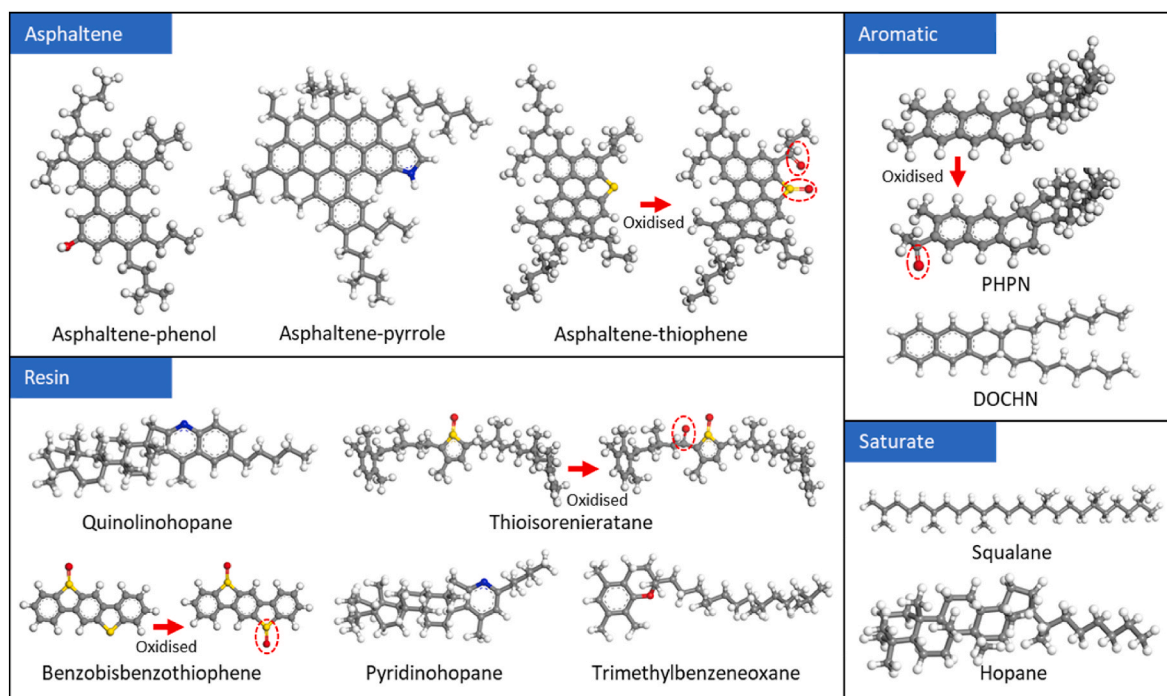


Fig. 1. Molecules of SARA fractions used for the virgin and aged PEN70/100 bitumen in this study. Hydrogen atoms are white, carbon atoms are grey, oxygen atoms are red, nitrogen atoms are blue, and yellow are sulphur atoms. (For interpretation of the references to colour in this figure legend, the reader is referred to the Web version of this article.)

**Table 2**  
Chemical composition of molecular models for the virgin and aged bitumen.

SARA fractions	Molecules in model	Molecular formula	Virgin bitumen			Aged bitumen		
			NM <sup>a</sup>	FWM <sup>b</sup> (wt%)	FWB <sup>c</sup> (wt%)	NM <sup>a</sup>	FWM <sup>b</sup> (wt%)	FWB <sup>c</sup> (wt%)
Saturate	Squalane	C <sub>30</sub> H <sub>62</sub>	16	3.9	3.6	16	3.8	3.6
	Hopane	C <sub>35</sub> H <sub>62</sub>	8			8		
Aromatic	PHPN	C <sub>35</sub> H <sub>44</sub>	160	52.3	53.3	96	43.7	43.9
	Oxidised PHPN	C <sub>35</sub> H <sub>42</sub> O	0			48		
Resin	DOCHN	C <sub>30</sub> H <sub>46</sub>	168			136		
	Quinolinoxane	C <sub>40</sub> H <sub>59</sub> N	24	31.0	30.3	32	33.8	33.9
	Thioisorenieratane	C <sub>40</sub> H <sub>60</sub> SO	24			0		
	Oxidised thioisorenieratane	C <sub>40</sub> H <sub>58</sub> SO <sub>2</sub>	0			24		
	Benzobisbenzothiophene	C <sub>18</sub> H <sub>10</sub> S <sub>2</sub> O	104			0		
	Oxidised benzobisbenzothiophene	C <sub>18</sub> H <sub>10</sub> S <sub>2</sub> O <sub>2</sub>	0			104		
	Pyridinohopane	C <sub>36</sub> H <sub>57</sub> N	24			32		
Asphaltene	Trimethylbenzeneoxane	C <sub>29</sub> H <sub>50</sub> O	32			32		
	Asphaltene-phenol	C <sub>42</sub> H <sub>54</sub> O	16	12.7	12.8	24	18.8	18.6
	Asphaltene-pyrrole	C <sub>66</sub> H <sub>81</sub> N	16			24		
	Asphaltene-thiophene	C <sub>51</sub> H <sub>62</sub> S	16			0		
	Oxidised asphaltene-thiophene	C <sub>51</sub> H <sub>60</sub> SO <sub>2</sub>	0			24		

<sup>a</sup> NM, number of molecules.

<sup>b</sup> FWM, fraction weight in the model.

<sup>c</sup> FWB, fraction weight in experimental bitumen.

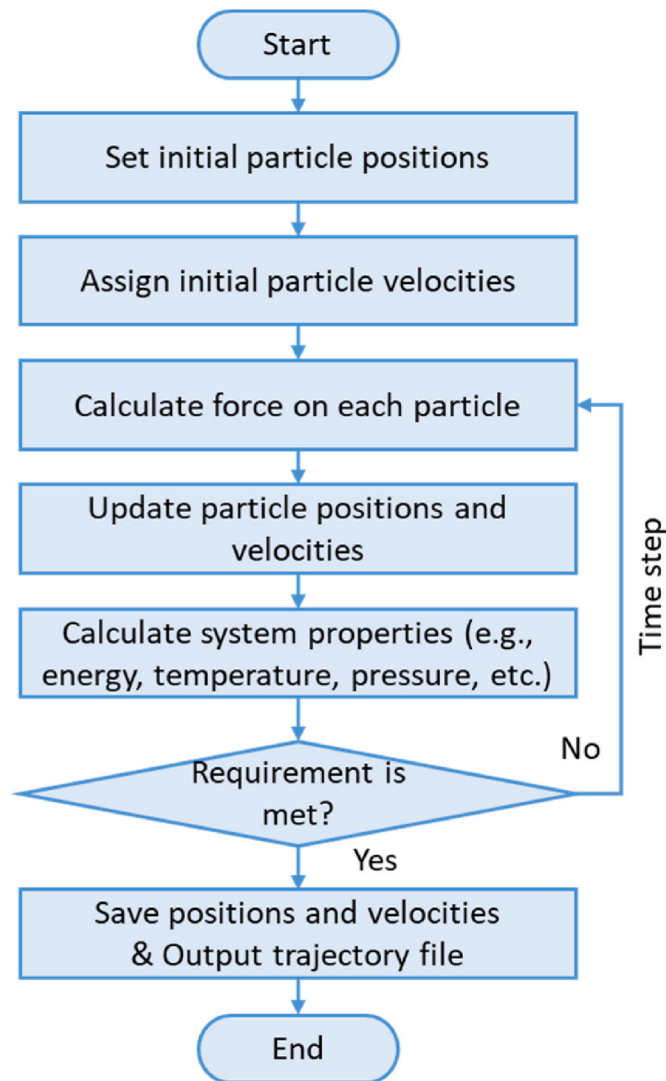


**Fig. 2.** Flow chart for calculation in MD simulations.

### 2.3.2. Force field

An essential input to MD simulations is the force field (interatomic potential) that computes the forces among the atoms. In this study, the interactions between the atoms in the molecular models of the virgin and aged bitumen are described by the Condensed-phase Optimized Molecular Potentials for Atomistic Simulation Studies (COMPASS) force field [42]. The COMPASS is a widely parameterised and validated force field and has been applied for MD simulations of bitumen materials [43–45].

The total potential energy ( $E_{total}$ ) in the COMPASS force field can be divided into the valence energy ( $E_{valence}$ ) and the non-bond energy ( $E_{non-bond}$ ), as shown in Eq. (2).

$$E_{total} = E_{valence} + E_{non-bond} \quad (2)$$

The valence term consists of the interaction energy caused by bond ( $E_b$ ), angle ( $E_a$ ), dihedral ( $E_d$ ) and improper ( $E_i$ ), as expressed in Eq. (3).

$$E_{valence} = E_b + E_a + E_d + E_i \quad (3)$$

The bond energy can be calculated by Eq. (4).

$$E_b = \sum_{n=2}^4 k_n^b (b - b_0)^n \quad (4)$$

where  $b_0$  is the equilibrium bond distance and  $k_n^b$  is the  $n$ th bond coefficient.

The angle energy includes the angle, bond-bond, and bond-angle terms, which can be obtained by Eqs. (5)–(8).

$$E_a = E^a + E^{bb'} + E^{ba} \quad (5)$$

$$E^a = \sum_{n=2}^4 k_n^a (\theta - \theta_0)^n \quad (6)$$

$$E^{bb'} = k^{bb'} (b - b_0)(b' - b'_0) \quad (7)$$

$$E^{ba} = k_1^{ba} (b - b_0)(\theta - \theta_0) + k_2^{ba} (b - b'_0)(\theta - \theta_0) \quad (8)$$

where  $\theta_0$  is the equilibrium angle and  $k_n^a$ ,  $k^{bb'}$  and  $k^{ba}$  are the coefficients for the angle, bond-bond, and bond-angle terms, respectively.

The dihedral energy contains the dihedral angle, bond-torsion, angle-torsion, and angle-angle-torsion terms, which are given by Eqs. (9)–(13).



$$E_d = E^t + E^{bt} + E^{at} + E^{aat} \quad (9)$$

$$E^t = \sum_{n=1}^3 k_n' [1 - \cos(n\varphi - \varphi_n)] \quad (10)$$

$$E^{bt} = (b - b_0) \sum_{n=1}^3 k_n^{bt} \cos n\varphi \quad (11)$$

$$E^{at} = (\theta - \theta_0) \sum_{n=1}^3 k_n^{at} \cos n\varphi \quad (12)$$

$$E^{aat} = k^{aat} (\theta - \theta_0) (\theta' - \theta_0') \cos \varphi \quad (13)$$

where  $\varphi$  is the torsional angle defined by the quadruplet of atoms and  $k$  is the corresponding coefficient.

The angle energy involves the improper and angle-angle terms, which are defined by Eqs. (14)–(16).

$$E_i = E^o + E^{aa'} \quad (14)$$

$$E^o = k^o (\chi - \chi_0)^2 \quad (15)$$

$$E^{aa'} = k^{aa'} (\theta - \theta_0) (\theta' - \theta_0') \quad (16)$$

where  $\chi_0$  is the equilibrium out-of-plane angle.

The non-bond term is composed of van der Waals energy ( $E^{vdw}$ ) and electrostatic energy ( $E^{elec}$ ), as described in Eq. (17). The van der Waals energy ( $E^{vdw}$ ) is written in the form of a Lennard-Jones (LJ) 9–6 function shown in Eq. (18), while the electrostatic energy ( $E^{elec}$ ) is represented by a standard Coulombic interaction with partial atomic charges shown in Eq. (19) [42].

$$E_{non-bond} = E^{vdw} + E^{elec} \quad (17)$$

$$E^{vdw} = \varepsilon \left[ 2 \left( \frac{r^0}{r} \right)^9 - 3 \left( \frac{r^0}{r} \right)^6 \right] \quad (18)$$

$$E^{elec} = \frac{q_i q_j}{r_{ij}} \quad (19)$$

where  $\varepsilon$  is the coefficient of well-depth energy,  $r$  is the distance between atoms,  $r^0$  is the distance where the LJ potential is zero, and  $q_i$  and  $q_j$  are the partial charges on atoms  $i$  and  $j$ , respectively.

Table 3 presents all the terms and their coefficients of interatomic potentials used in the virgin and aged bitumen systems. The simulation system contains 44,728 atoms for the virgin bitumen but 47,048 atoms for the aged bitumen. All the types and their coefficients of bond, angle, dihedral and improper in the systems were defined by the COMPASS force field.

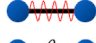
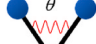


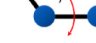







### 2.3.3. Model construction and dynamic equilibrium

The molecular models of the virgin and aged bitumen were built and equilibrated by the following procedure of MD modelling and simulations.

- (1) The 3D atomic configuration of the individual molecules (see Table 2) used for the bitumen models was created by using its corresponding SMILES [46] notation. An energy minimization step was followed to generate a relatively stable conformer.
- (2) The individual molecules were homogeneously placed in an elongated simulation box with a low density of 0.25 g/cm<sup>3</sup> to initialize the molecular positions in the bitumen models. The molecules were distributed using a quasi-random Sobol distribution method so that they were spread and rotated more evenly and not overlapped.

**Table 3**

Types and their coefficients of interatomic potentials in the bitumen system.

No	Terms			Coefficients
1		Bond	Eq. (4) bond	$b_0, k_1^b, k_2^b, k_3^b$
2		Angle	Eq. (6) angle	$\theta_0, k_1^a, k_2^a, k_3^a$
3			Eq. (7) bond-bond	$k^{bb}, b_0, b_0'$
4			Eq. (8) bond-angle	$k_1^{ba}, k_2^{ba}, b_0, b_0'$
5		Dihedral	Eq. (10) dihedral angle	$k_1^d, k_2^d, k_3^d, \varphi_1, \varphi_2, \varphi_3$
6			Eq. (11) bond-torsion	$b_0, k_1^{bt}, k_2^{bt}, k_3^{bt}$
7			Eq. (12) angle-torsion	$\theta_0, k_1^{at}, k_2^{at}, k_3^{at}$
8		Improper	Eq. (13) angle-angle-torsion	$k^{aat}, \theta_0, \theta_0'$
9			Eq. (15) improper	$k^o, \chi_0$
10			Eq. (16) angle-angle	$k^{aa}, \theta_0, \theta_0'$
11		van der Waals	Eq. (18) van der Waals	$\varepsilon, r^0$
12		Electrostatics	Eq. (19) Electrostatics	N/A

- (3) The COMPASS force field types and charges were assigned to the system. The particle positions in the system were optimized to ensure that they accommodated lower energy configurations in response to the newly assigned force field.
- (4) The system was compressed by shortening the length of the box in the z-direction until it reached its target density. Simulation details to determine the target density of the bitumen model can be found in the authors' previous work [37].
- (5) An NPT (N, constant number of atoms; P, constant pressure; and T, constant temperature) dynamics simulation with full periodic boundary conditions was run for 500 ps (ps) at a temperature of 298 K and a pressure of 1 atm.
- (6) An NVT dynamics simulation where the system volume (V) and temperature (T) are controlled was performed for 5 ns (ns) to further relax and equilibrate the bitumen system. The resulting bitumen system was well mixed and its system properties such as energy did not change further over time.

The equilibrated bitumen model has a size of  $47 \times 47 \times 200$  Å in the x, y, and z directions. Fig. 3 shows an equilibrated model of the virgin bitumen. In this study, all the molecular dynamics simulations were run using LAMMPS [47].

### 2.4. MD tensile simulations

Following the equilibration process mentioned in Section 2.3.3, a tensile simulation was performed at the temperature of 293 K (i.e., 20 °C) to determine the fracture strength of bitumen at the molecular scale. Equibiaxial strain-controlled tensile loading was applied for an equilibrated bitumen model by dilating the simulation box along the z-direction at a constant strain rate of  $10^9$ /s. The strain rate was adopted considering the balance between the accuracy of simulation results and computational time cost. It should be noted that this strain rate has been applied previously for MD simulations of both bitumen [30] and polymer [48] materials. An isothermal NVT ensemble was used during the tensile simulation.

The stress tensor of individual atoms in the bitumen system was defined by Eq. (20) [49,50]. The first term represents the kinetic energy contribution due to atomic motion, which is related to temperature. The

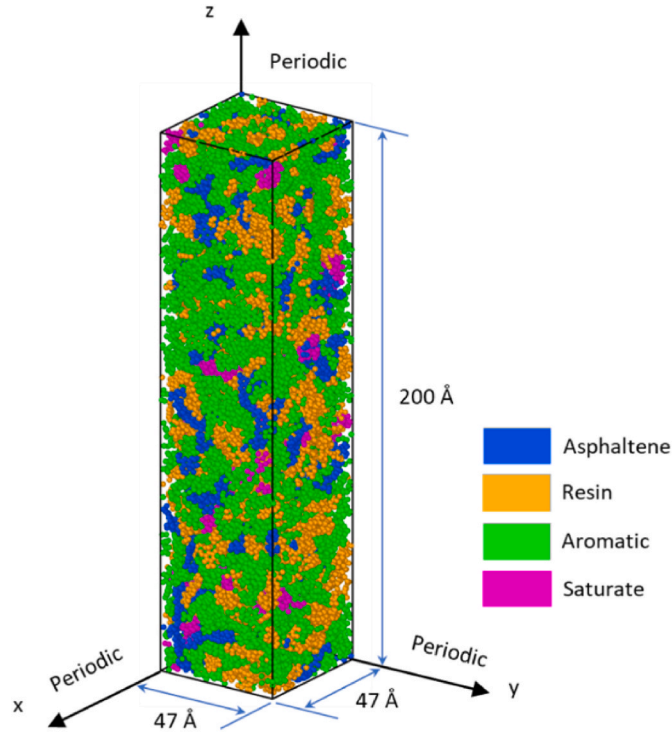


Fig. 3. An equilibrated model of the virgin bitumen used for the tensile and fatigue simulations.

second term is the virial contribution associated with intramolecular and intermolecular interactions, which is related to interatomic forces governed by the force field described in Section 2.3.2. The per-atom stress tensor is a stress\*volume formulation. The total stress values of the bitumen system in the loading (z) direction can be obtained by the sum of the z components of the per-atom stress tensor for all atoms in the system divided by the volume of the system. The strain of the bitumen system in the loading (z) direction was calculated by the ratio between the deformation/elongation and the original size of the simulation system in the z dimension and recorded to obtain the stress-strain response of the system.

$$\sigma_{\alpha\beta} = -mv_{\alpha}v_{\beta} - \frac{1}{2} \sum_{n=1}^N (r_{\alpha}F_{\beta}) \quad (20)$$

where  $\alpha$  and  $\beta$  take on x, y, or z for the components of the tensor,  $m$  is the mass of the atom,  $v$  is the velocity of the atom,  $N$  is the number of atoms for atomic interaction,  $r$  is the vector between the positions of two atoms, and  $F$  is the interaction force between two atoms.

## 2.5. MD fatigue simulations

A strain-controlled fatigue simulation was conducted at a temperature of 293 K using an isothermal NVT ensemble, which includes two major processes: (1) a quick tensile simulation and (2) a sinusoidally oscillatory simulation. The equilibrated bitumen model was first subjected to an equibiaxial tensile load with a strain rate of  $10^9/s$  to obtain an initial mean strain. The mean strain must be less than the fracture strain of the bitumen obtained from the tensile simulation shown in Section 2.4. After that, fatigue loading was applied by sinusoidally stretching and compressing the simulation box in the z-direction using Eq. (21) [51]. A loading period of 1ps was chosen for the fatigue simulation, based on its previous use for MD simulations of polymer materials [52,53]. It should be noted that in MD simulations, the time scale is in the nanosecond (ns) range. Due to the restriction of computational time cost, the simulation in this study was focused on low cycle

(500 cycles) fatigue to investigate the essential mechanistic features at the early (initiation) stage of fatigue damage in the bitumen.

$$L_t = L_0 + a \sin\left(\frac{2\pi t}{T}\right) \quad (21)$$

where  $L_t$  is the box length in the z-direction at any time  $t$  during the fatigue simulation,  $L_0$  is the box length immediately after applying the tensile mean strain,  $a$  is the amplitude, and  $T$  is the loading period.

In this study, MD simulations were performed using the Large-scale Atomic/Molecular Massively Parallel Simulator (LAMMPS) programme [47]. A time step of 1 fs (fs) and a cut-off distance of 9.5 Å were applied for all the simulations. During the simulation, the temperature of the system was controlled by the Nosé-Hoover thermostat. The atomic trajectories of the simulation process were viewed using the visualisation tool OVITO [54]. A flowchart of the main MD modelling and simulations in this study is shown in Fig. 4.

## 2.6. Dynamic shear rheometer (DSR) tests

The fatigue behaviours of bitumen at the macroscale were characterised in the laboratory by using a dynamic shear rheometer (DSR) (TA-HR1, TA Instruments Company, USA). Bitumen samples with a diameter of 8 mm (2 mm in height) were prepared for the DSR-based fatigue tests. Fig. 5 illustrates the main configuration of DSR testing. The fatigue tests were conducted on the virgin and aged bitumen samples at an intermediate temperature. Specifically, time sweep tests with a 5% strain level were carried out at a temperature of 20 °C and a frequency of 10 Hz. The strain level has been used to evaluate the fatigue resistance of bitumen modified anti-ageing compounds [55]. The complex shear moduli and phase angles of the samples were recorded during the full duration of the fatigue testing. Fig. 6 shows the results of the time sweep tests for the virgin and aged bitumen. It is noted that the initial experimental data for the first 50 cycles (5 s) were not used as the test machine had not reached the steady state of the strain level (5%).

## 3. Results and discussion

### 3.1. Model validation

To validate the developed molecular models for the virgin and aged bitumen, the thermodynamic properties of the bitumen models were calculated and compared with the experimental and reference results, including density, cohesive energy density (CED), and the solubility parameter. The MD simulation details for predicting these thermodynamic properties of the bitumen models can be found in the authors' previous work [37]. Table 4 shows the predicted results for the virgin and aged bitumen models. It is found that the predicted results are very close to the experimental and reference data. Furthermore, the tensile simulation results of the bitumen models in Section 3.2 exhibit a non-linear behaviour, indicating the bitumen's viscoelastic characteristic. In addition, the stress-strain response of the bitumen system in one loading cycle was analysed and shown in Fig. 7. A hysteresis loop can be seen in the stress-strain curve, which indicates the rheological behaviour of the bitumen. Therefore, the proposed bitumen models and MD simulations based on the COMPASS are able to describe the thermodynamic properties of the bitumen and can be further applied for the investigation into the fatigue behaviours of bitumen at the molecular scale.

### 3.2. Tensile simulations

Fig. 8 presents the mechanical behaviours of the virgin and aged bitumen under tensile loading. The stress-strain response in the tensile simulation is depicted in Fig. 8(a). Fig. 8(b) shows snapshots capturing the bitumen deformation corresponding to 5 points marked in the stress-separation curves. Following a linear increase (from point A to point B),

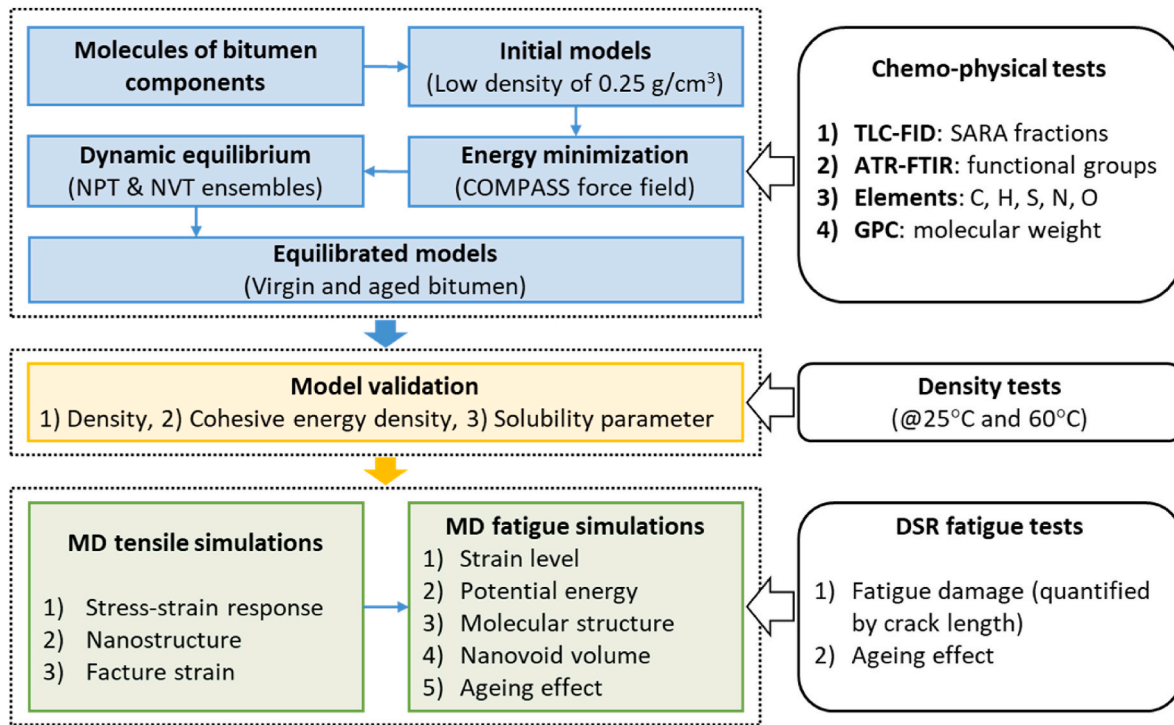


Fig. 4. Flowchart of MD modelling and simulations in this study.

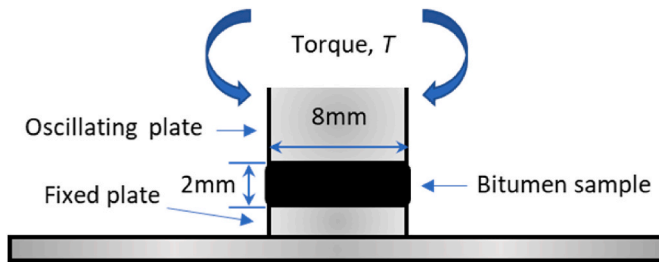


Fig. 5. DSR testing configuration with a bitumen sample.

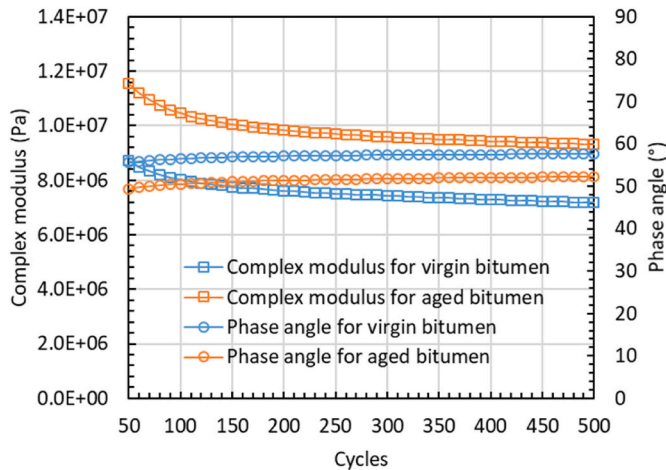


Fig. 6. Complex modulus and phase angle of the virgin and aged bitumen obtained from time sweep tests.

the tensile stress exhibits a nonlinear increase (from point B to point C) with the increasing strain until it reaches a peak value (the maximum stress). With further stretched, nanovoids (cavities) can be observed in

the bitumen, as shown in Fig. 8(b). The stress shows a gradual decrease (from point C to point D) and then drops sharply (from point D to point E) until it approaches zero (or a very small value) in the end. It can be seen from Fig. 8(a) that the virgin and aged bitumen experience the same trend in terms of the stress-strain curves. However, before the peak value, the stress-strain curve of the aged bitumen has a larger slope than that of the virgin bitumen, which indicates a higher modulus (see Fig. 6). This is because the physical hardening happens during oxidative ageing due to the introduction of oxygen atoms, which has been reported by previous experimental [38] and simulation [59] studies.

In the stress-strain curve, the maximum stress is defined as the fracture strength and the corresponding strain is the fracture strain. It is also seen in from Fig. 8(a) that the virgin and aged bitumen have nearly the same fracture strength. However, the fracture strain (11.6%) of the aged bitumen is slightly smaller than that (12.2%) of the virgin bitumen. According to the results of tensile simulations, the strain levels that are less than the fracture strains were selected for the following fatigue simulations of the virgin and aged bitumen.

### 3.3. Fatigue damage characterisation based on MD simulations

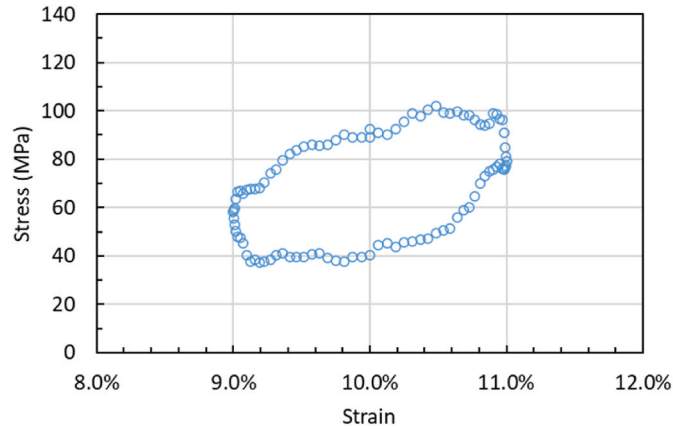
#### 3.3.1. Effect of strain levels

To investigate the effect of strain levels on the fatigue behaviours of bitumen, different mean strains and amplitudes were applied in fatigue simulations. The mean strains of 5%, 7%, and 10% with an amplitude of 2 Å were used for the virgin bitumen model, which were smaller than the fracture strain of bitumen shown in Fig. 8(a). Fig. 9(a) presents the stress responses to three applied mean strains during fatigue simulations. It is observed that the stress corresponding to the mean strain of 10% is larger than that corresponding to the mean strain of 7% or 5%. This indicates that the mean strain has a significant effect on the stress response in the fatigue simulation. When a higher mean strain is applied, the corresponding stress will be larger. This finding is consistent with the previous study, in which Sahputra and Echtermeyer [52] reported that the stress increased with the increasing mean strain level in terms of the fatigue behaviour of amorphous polyethylene at the molecular scale. Furthermore, it is observed from Fig. 9(a) that three mean strains have a

**Table 4**

Predicted thermodynamic properties for the virgin and aged bitumen models compared with the experimental and simulation results.

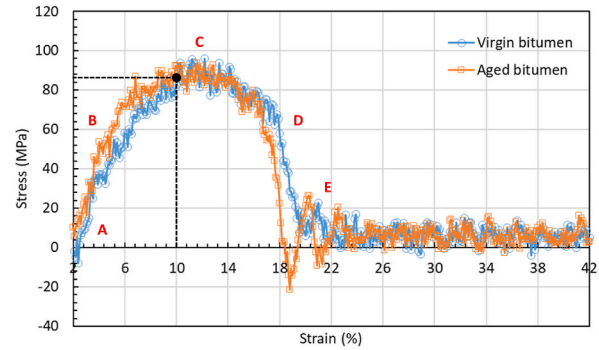
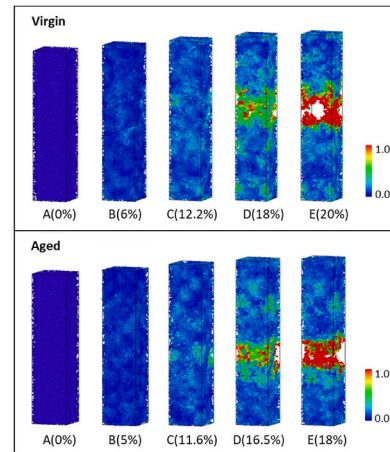
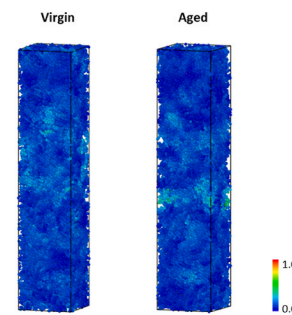
Property	Virgin bitumen		Aged bitumen		Reference data
	Simulation	Experiment	Simulation	Experiment	
Density @ 25 °C (g/cm <sup>3</sup> )	0.999	1.017	1.014	1.024	1.01–1.04 [56]
Density @ 60 °C (g/cm <sup>3</sup> )	0.984	0.996	1.003	1.003	
Cohesive energy density (10 <sup>8</sup> J/m <sup>3</sup> )	3.36	N/A	3.43	N/A	3.32, 3.59 [57]
Solubility parameter [(J/cm <sup>3</sup> ) <sup>-0.5</sup> ]	18.33	N/A	18.52	N/A	18.19 [58]

**Fig. 7.** Stress-strain response of the bitumen system in one loading cycle.

similar stress response process with the load cycles in fatigue simulations, although their stress levels were different. The stress gradually decreases with the increasing load cycles at the beginning of the simulation. This is due to the change of molecular structures (e.g., molecular rearrangement and nanovoid formation) in the bitumen model under fatigue loading. After the stress reaches a minimum value, it remains relatively stable with an increase in load cycles because of the lower atomic local strain under the strain-controlled fatigue load mode.

In addition, three displacement amplitudes of 0 Å (0% strain), 1 Å (0.5% strain) and 2 Å (1% strain) with a mean strain of 10% were used in fatigue simulations to study the effect of displacement amplitude. The displacement amplitudes of 1 and 2 Å correspond to 0.5% and 1% of the simulation box length in the z-direction, respectively. The displacement amplitude of 0 Å means that no oscillatory load was applied to the simulation model and the mean strain was kept at a constant level (10%) during the simulation. Fig. 9(b) presents the stress responses to the applied mean strain of 10% with three displacement amplitudes during fatigue simulations. It can be seen that, for all three applied displacement amplitudes, the stress first decreases gradually and then remains stable with the increasing load cycles. When the displacement amplitude is 0 Å, the reduction of stress is known as stress relaxation, which indicates the viscoelastic characteristic of bitumen. For the displacement amplitudes of 1 and 2 Å, the decreasing stress is caused by stress relaxation, fatigue damage or both. Moreover, it is found from Fig. 9(b) that the stress corresponding to the displacement amplitude of 2 Å is smaller than that corresponding to the displacement amplitude of 1 or 0 Å in the first 200 load cycles, which means that increasing the displacement amplitude leads to more severe damage of bitumen. However, the three displacement amplitudes have almost the same stress in the last 300 cycles due to the lower atomic local strain in the strain-controlled load mode.

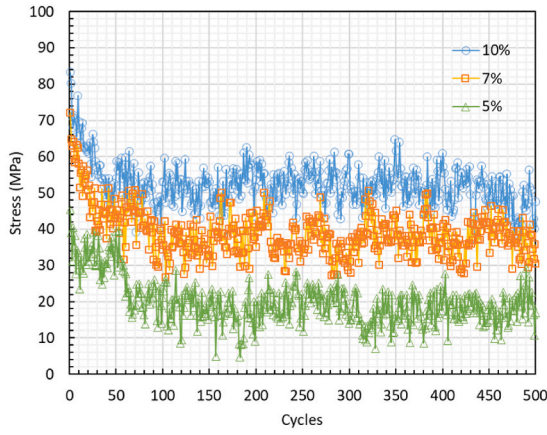
In this study, considering the limitation of computation time cost, the large strain of 10% with the displacement amplitude of 2 Å was used for fatigue simulations. A snapshot at the strain of 10% coloured by the atomic local shear strain is presented in Fig. 8(c), where no nanovoids have been formed yet and the significant local strain is not observed in the bitumen.

**(a)** The stress-strain response in the tensile simulation.**(b)** Snapshots capturing the bitumen deformation at different strain levels. Colour indicates the atomic local shear strain.**(c)** A snapshot of bitumen deformation at the strain of 10%.**Fig. 8.** Mechanical behaviours of the virgin and aged bitumen under tensile loading.

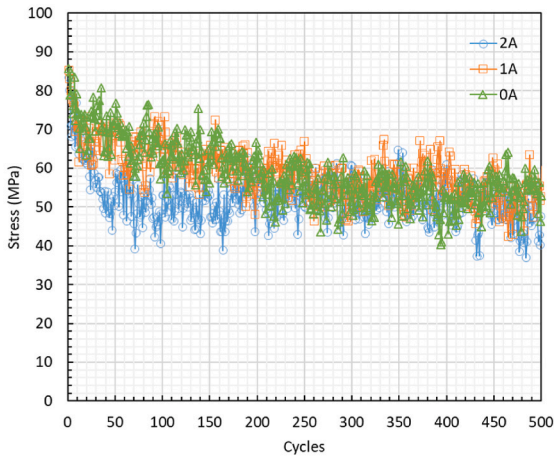
### 3.3.2. Potential energy

To understand the molecular behaviours leading to bitumen fatigue damage, the potential energies in the simulation system were calculated and analysed based on the force field equations shown in Section 2.3.2.





(a) Different mean strain levels with a displacement amplitude of 2 Å.



(b) Different displacement amplitudes with a mean strain of 10%.

Fig. 9. Stress response with load cycles.

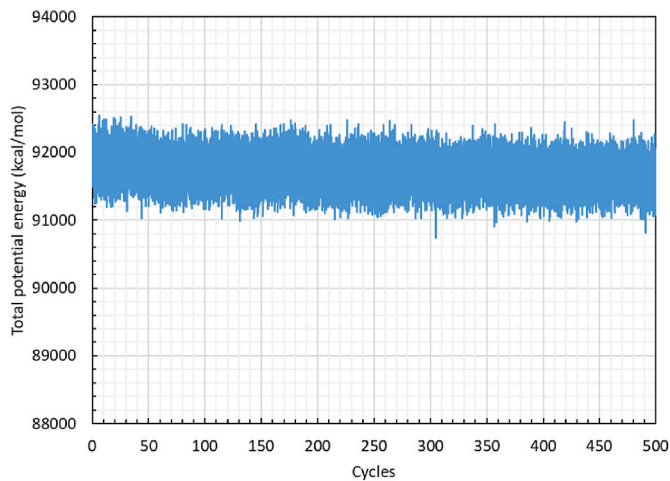


Fig. 10. Total potential energy in the bitumen during the fatigue simulations.

Fig. 10 presents the evolution in the total potential energy of the bitumen system during fatigue simulations for a typical case: a mean strain of 10 % with an amplitude of 2 Å. It can be seen that the total energy gradually decreases with the increasing load cycles, which

demonstrates that the molecular structures in the bitumen change under fatigue loading. As described in Section 2.3.2, the total potential energy is related to the intramolecular interactions (i.e., bond, angle, dihedral and improper) and the intermolecular interactions (i.e., van der Waals and Coulombic).

Fig. 11 shows the individual potential energies contributing to total potential energy in the bitumen during fatigue simulations. It is observed from Fig. 11(a)–(d) that all the intramolecular potential energies caused by bond, angle, dihedral and improper have no significant change in magnitudes during the whole simulation. The intermolecular potential energies including van der Waals and Coulombic interactions decrease with an increase in load cycles, as presented in Fig. 11(e) and (f), which lead to the decreasing total potential energy in the simulation system. This is because the intermolecular interactions produce weaker forces compared to the intramolecular interactions binding the monomers in the bitumen molecules. The decrease of intermolecular potential energies was also found in the amorphous polyethylene [52] and epoxy composites [60] under fatigue loading.

The intermolecular interactions (i.e., van der Waals and Coulombic forces) are related to the distance between molecules, as shown in Eq. (18) and (19). The negative values represent the attractive forces that bind the molecules together in the bitumen system. It is found from Fig. 11(e) and (f) that the magnitude of their potential energies shows an increasing trend with the increasing number of load cycles. This indicates a reduction of distance between bitumen molecules in the entire simulation system due to molecular rearrangement in the bitumen under fatigue loading. When the bitumen is subjected to a fatigue load, the molecules in the bitumen align themselves in the load direction and get closer to each other. This will be further proved by the molecular structure analysis in the following section.

### 3.3.3. Molecular structure

To further study the molecular behaviours of bitumen under fatigue loading, the molecular structure in the bitumen was analysed by using a radius of gyration. The radius of gyration is defined as the root mean square distance between the mass centre of the molecule and each atom position in this molecule, as shown in Eq. (22). This parameter implies the level of compaction or how folded or unfolded the molecular chains are. Fig. 12 shows the radius of gyration along the loading direction in the bitumen during the fatigue simulations. It can be seen that the radius of gyration increases as the load cycles increase, especially in the first 50 load cycles, which indicates that the bitumen molecules become unfold and tend to align along the loading direction when fatigue loading is applied. The change in the molecular configuration helps the molecular chains move closer together and thus contributes to the reduction of the intermolecular interactions including the van der Waals and Coulombic energies shown in Fig. 11(e) and (f). Based on small-angle neutron scattering (SANS) data, it has been found that the radius of gyration of polymer materials (e.g., a linear polyethylene film) increases along the loading direction at room temperature [61].

$$R_g^2 = \frac{1}{M} \sum m_i (r_i - r_{cm})^2 \quad (22)$$

where  $M$  is the total mass of the molecule,  $r_i$  is the mass of atom  $i$ ,  $r_{cm}$  is the mass centre of the molecule, and the sum is over all atoms in the molecule.

### 3.3.4. Formation and growth of nanovoids

In addition to the stress-strain response, potential energy and molecular structure, the molecular behaviours of bitumen during fatigue simulation were further analysed to understand the damage mechanism of bitumen under fatigue loading. Fig. 13 illustrates a sequence of snapshots capturing the nanostructure of bitumen during the fatigue simulation. It can be seen that small nanovoids first appeared in the bitumen and then gradually grew with the increasing load cycles. These

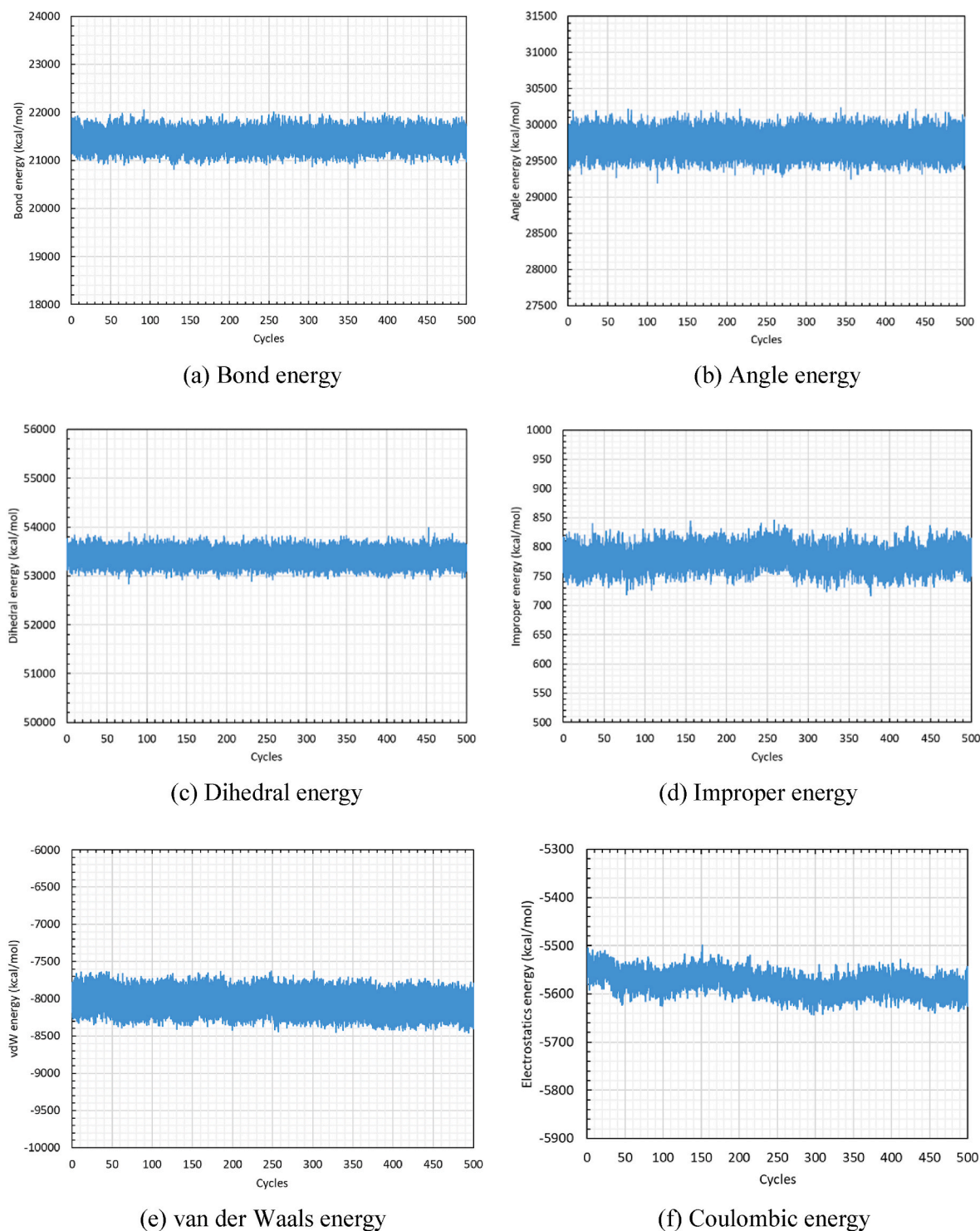


Fig. 11. Individual potential energy in the bitumen during the fatigue simulations.

nanovoids are the areas without any molecules, which are caused by the movement and rearrangement of molecules in the model under fatigue loading.

In Fig. 13, only nanovoids connected to both the front and back surfaces can be viewed in the model. To quantify the nanovoids inside the model, a surface mesh was established to reconstruct the geometric boundaries of a set of bitumen atoms. The surface mesh divides space into an atomistic solid and an open (empty) region shown in Fig. 14, which facilitates the measurements of the surface area and the solid volume in the bitumen's nanostructure. Using the alpha-shape method

[62], a virtual probe sphere with a radius of 4 Å is applied in this study to create a closed surface mesh for the nanostructure of the bitumen. Fig. 15 shows the established surface mesh for nanovoids in the bitumen under fatigue loading.

Fig. 16 presents the evolution of nanovoids in the bitumen with the increasing fatigue load cycles. It can be observed that the nanovoid size gradually increases with the increasing load cycles. The evolution of nanovoids resembles the increase of cavity size measured by using a near-infrared dark field microscope [20]. Based on the established surface mesh, the volume of nanovoids formed in the bitumen model was



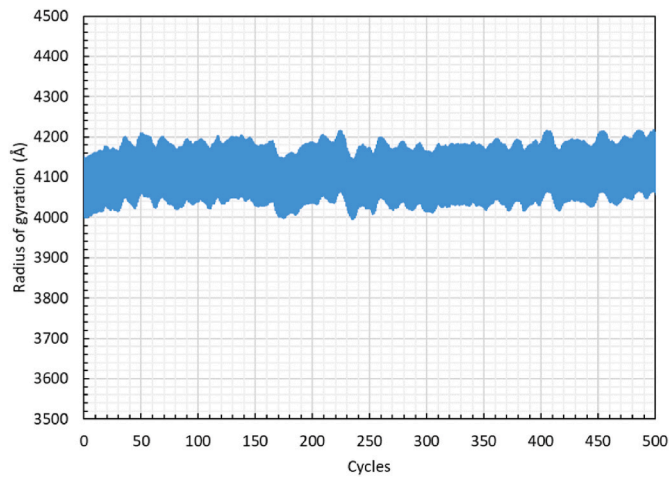


Fig. 12. Radius of gyration along the loading direction during the fatigue simulations.

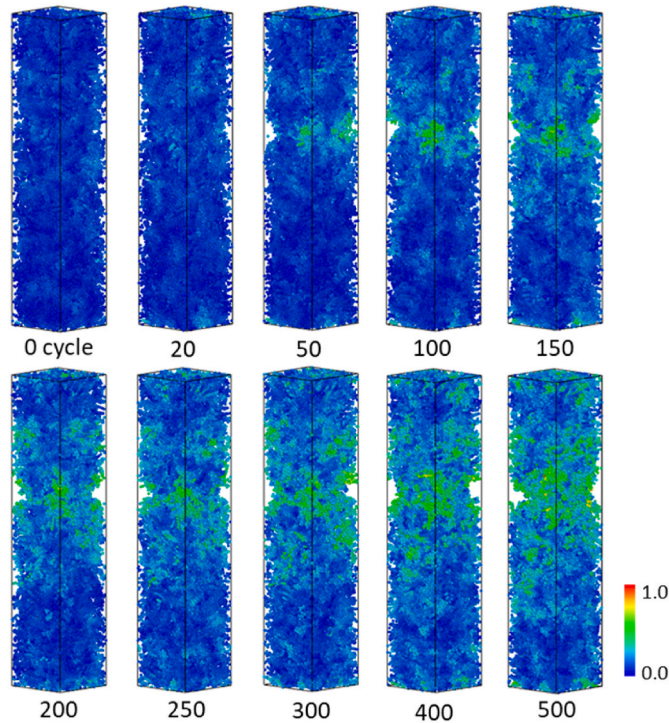


Fig. 13. A sequence of snapshots capturing the deformation and nanovoids of bitumen under fatigue loading. Colour indicates the atomic local shear strain. (For interpretation of the references to colour in this figure legend, the reader is referred to the Web version of this article.)

calculated to quantify the nanostructure changes of bitumen due to fatigue loading. Fig. 17 shows the nanovoid volume in the bitumen with the load cycles during the fatigue simulations. It can be seen that the nanovoid volume increases as the load cycle increases, which indicates that the fatigue loading results in the formation and growth of nanovoids through molecular rearrangement and movement in the bitumen. These nanovoids at the molecular scale will grow and nucleate into small microcracks and eventually cause fatigue damage (cracking) of bitumen at the macroscale. This is considered one of the most important molecular mechanisms leading to bitumen fatigue damage. The recently published work from Hajj et al. [63] examined the cyclic behaviour of bitumen under unidirectional loading. The fatigue damage behaviour of bitumen subjected to high amplitude cyclic loading was investigated

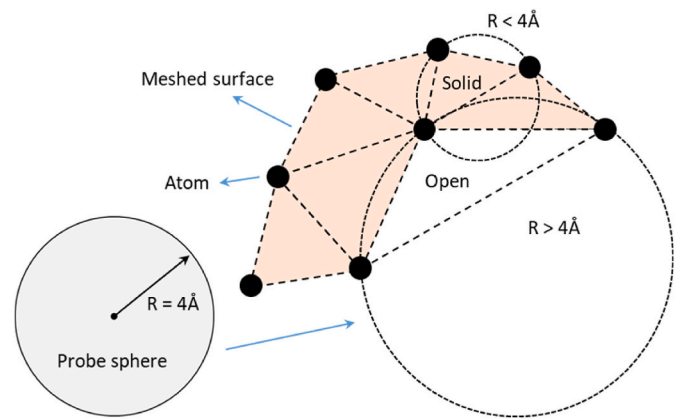


Fig. 14. Schematic for surface mesh establishment with a probe sphere.

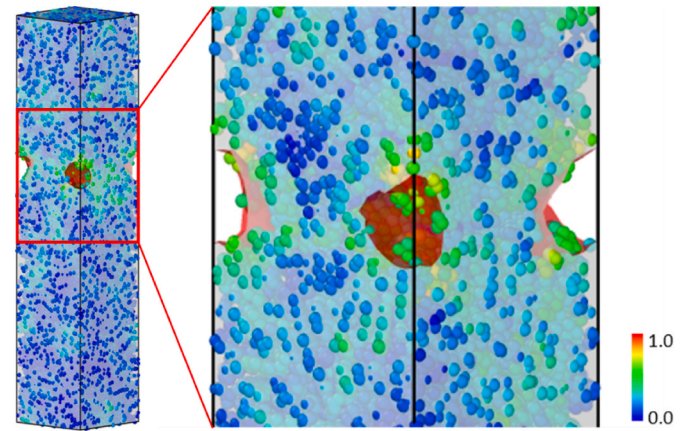


Fig. 15. Surface mesh for nanovoids in the bitumen under fatigue loading.

though observing its bulk microstructure using dark field optical microscopy. It was reported that the cavities could occur and grow in bitumen during the initial stage of material failure, which serve as nucleation sites for microcracks. Their observation of the cavitation is consistent with the simulation results in this study.

### 3.3.5. Effect of ageing

To investigate the effect of ageing on the fatigue performance of bitumen at the molecular scale, the proposed MD-based fatigue simulations were performed on the aged bitumen to analyse its stress-strain response, potential energy, molecular structure, and nanovoids characteristics.

Fig. 18 shows the stress response for the aged bitumen under the mean strain level of 10% with an amplitude of 2 Å. The results of the virgin bitumen are also presented in Fig. 18 to facilitate the comparison. It can be seen that the stress of the aged bitumen gradually decreases before the 300th load cycle and then remains stable in the last 200 cycles. This decreasing trend is similar to that of the virgin bitumen. However, in the first 300 cycles, the aged bitumen has higher stress values than the virgin bitumen. This is because the modulus of the aged bitumen is larger than that of the virgin bitumen (see Fig. 6) due to the physical hardening that happens during oxidative ageing. The higher stress is also observed for the aged bitumen in the tensile simulations shown in Fig. 7 (a). As the load cycle increases, the stress of the aged bitumen decreases until it reaches a relatively stable value at the 300th cycle. Finally, the stress of the aged bitumen is nearly the same as that of the virgin bitumen in the last 200 cycles. This demonstrates that the

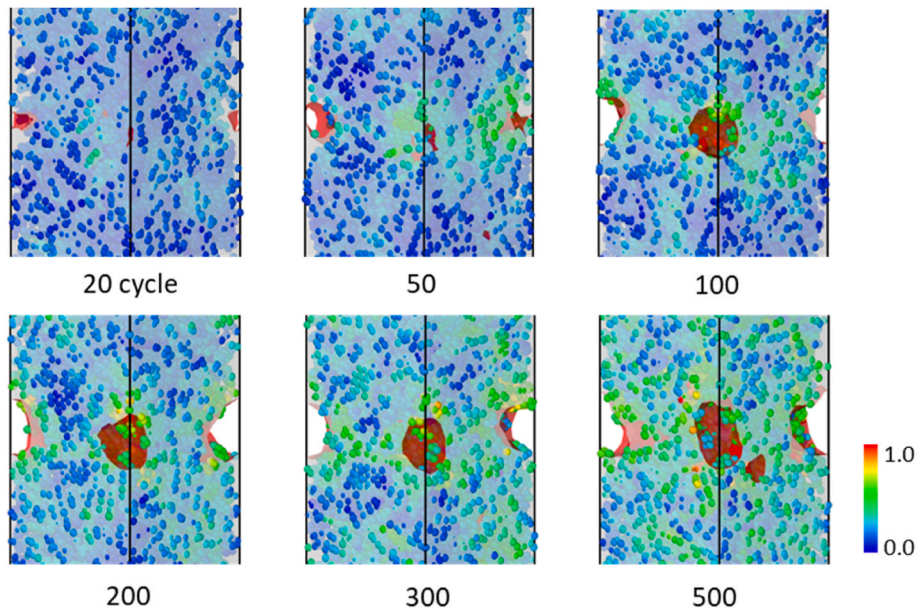


Fig. 16. Evolution of nanovoids in the bitumen with the increasing fatigue load cycles.

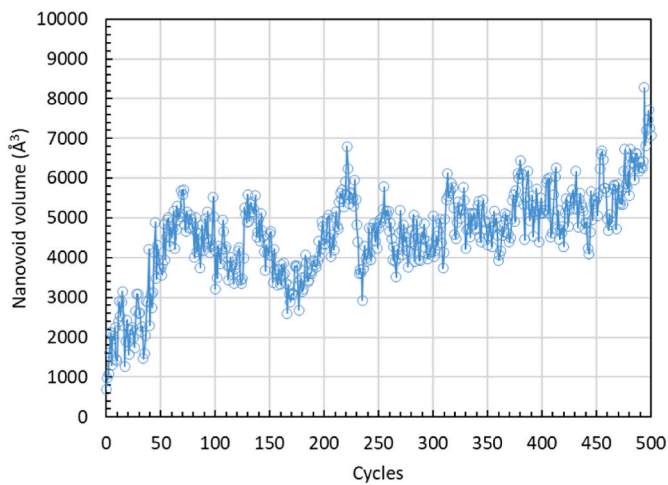


Fig. 17. Nanovoid volume in the bitumen under fatigue loading.

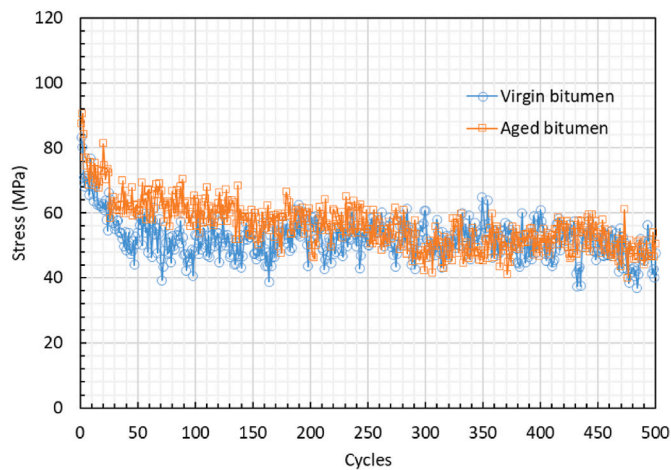


Fig. 18. Stress response for virgin and aged bitumen under the mean strain level of 10% with the amplitude of 2 Å.

aged bitumen produces more severe damage than the virgin bitumen, which can be further supported by their nanovoid volumes described later.

Based on the force field equations shown in Section 2.3.2, the total potential energy in the simulation system was calculated for the aged bitumen under a fatigue load with a mean strain of 10 % and an amplitude of 2 Å, as presented in Fig. 19. It can be seen that the total potential energy of the aged bitumen gradually decreases with an increase in load cycles, which is similar to that of the virgin bitumen. The decrease of total potential energy in the simulation system is caused by the decreasing intermolecular interactions (i.e., van der Waals and Coulombic) due to the molecular rearrangement in the aged bitumen after fatigue loading is applied. Furthermore, the change in the molecular structure of the aged bitumen during the fatigue simulation was quantified by using the radius of gyration, as shown in Fig. 20. It is found that the radius of gyration slightly increases with the increasing load cycles. This result indicates that the aged bitumen molecules tend to unfold and align along the loading direction under fatigue loading, which makes the molecules get closer to each other. This molecular movement contributes to the decrease of intermolecular interactions.

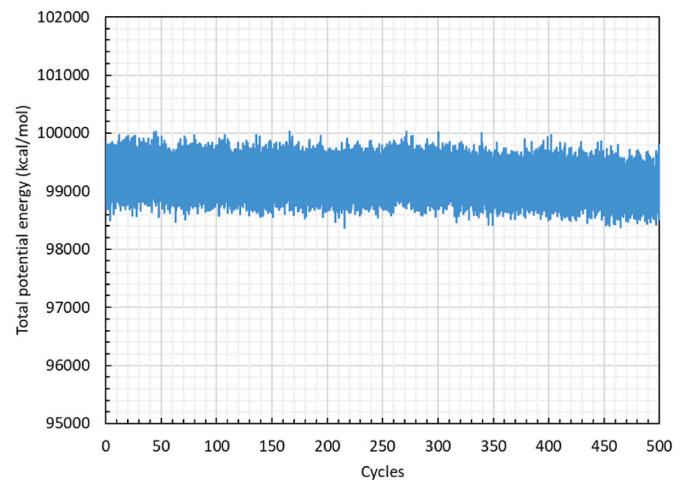


Fig. 19. Total potential energy in the aged bitumen during the fatigue simulations.



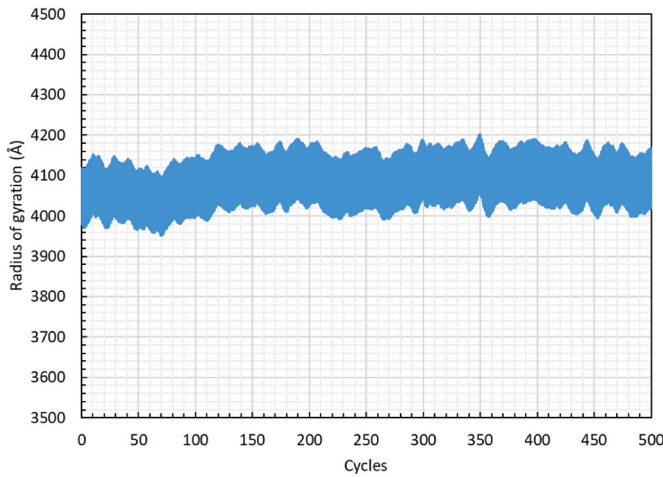


Fig. 20. Radius of gyration along the loading direction for the aged bitumen.

The nanostructure of the aged bitumen during the fatigue simulations was captured to fundamentally analyse the material damage under fatigue loading. Based on the nanostructure, the surface mesh was created to quantify the nanovoids inside the aged bitumen model. Fig. 21 shows the calculated nanovoid volume for the virgin and aged bitumen with the load cycles during the fatigue simulations. It is found that the nanovoid volume of the aged bitumen significantly increases in the first 300 load cycles and then the rate of increase decreases in the last 200 cycles. This indicates that the damage happens and grows in the aged bitumen due to molecular rearrangement and movement under fatigue loading. It should be noted that a strain-controlled model was applied for fatigue loading in this study. Therefore, with the increasing of load cycles, the damage in the material causes a drop of the stress shown in Fig. 18. When the stress decreases to a minimum value and then remains stable, the increasing rate of the damage indicated by the nanovoid volume will decelerate in the aged bitumen. Moreover, it can be seen from Fig. 21 that the aged bitumen has a higher nanovoid volume than the virgin bitumen, which demonstrates that the fatigue damage of the aged bitumen is more severe under the same fatigue loading. This finding is also supported by the results of the stress-strain response shown in Fig. 18, which will be further proved by the experimental results from the following DSR-based fatigue tests.

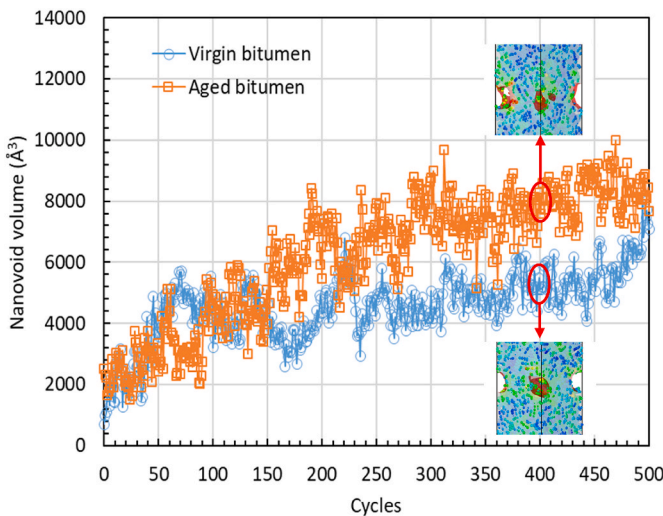


Fig. 21. Evolution of nanovoid volume in the virgin and aged bitumen under fatigue loading.

### 3.4. Fatigue damage characterisation based on DSR tests

The fatigue damage of the virgin and aged bitumen at the macroscale was characterised by time sweep tests using a dynamic shear rheometer (DSR). It has been found that the fatigue damage in the bitumen sample is a circumferential ‘edge crack’ under a DSR-based fatigue load [11–13]. Fig. 22(a) presents a typical crack surface morphology of a bitumen sample. This type of crack starts at the periphery of a sample and propagates towards the centre of the sample to generate a rough crack surface with radial peaks and valleys. Fig. 22(b) shows a schematic of the bitumen sample with a circumferential crack.

In this study, the fatigue crack of the virgin and aged bitumen was quantified by using a DSR-based cracking (DSR-C) model. The DSR-C model was developed based on damage mechanics in the authors’ previous work [13–15,64]. The fatigue crack length of bitumen in the model was defined and calculated by shear moduli and phase angles of the samples in the undamaged and damaged conditions, as described in Eq. (23). The shear modulus ( $|G_N^*|$ ) and the phase angle ( $\delta_N$ ) at the  $N$ th load cycle in the damaged condition were obtained from the time sweep tests. The initial values in the tests were selected as the undamaged shear modulus ( $|G_0^*|$ ) and the phase angle ( $\delta_0$ ). It should be noted that the DSR-C model has been validated and applied for unmodified and modified bitumen at different temperatures, frequencies and strain levels in previous work [13].

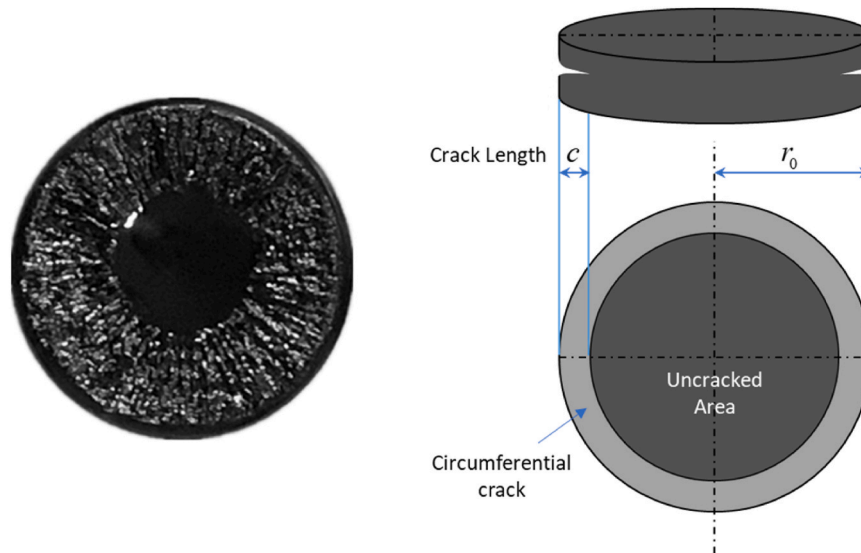
$$c = \left[ 1 - \left( \frac{|G_N^*|/\sin(\delta_N)}{|G_0^*|/\sin(\delta_0)} \right)^{\frac{1}{4}} \right] r_0 \quad (23)$$

where  $c$  is the fatigue crack length in the bitumen sample;  $r_0$  is the original radius of the bitumen sample;  $|G_0^*|$  and  $\delta_0$  are the undamaged shear modulus and phase angle, respectively; and  $|G_N^*|$  and  $\delta_N$  are the damaged shear modulus and phase angle at the  $N$ th load cycle, respectively.

Based on the DSR-C model shown in Eq. (23), the crack growth in the bitumen sample was analysed during the fatigue testing. Fig. 23 shows the crack growth curves of the virgin and aged bitumen under a DSR-based fatigue load. The initial experimental data for the first 50 cycles (5 s) were not used for the figure characterisation because the test machine had not reached the steady state of the strain level (5%). It can be found that the crack length exhibits a significant increase at the initial stage of the crack growth and then a relatively slow growth with the increasing number of load cycles. This increasing trend of the crack length at the macroscale is similar to that of the nanovoid volume at the molecular scale shown in Fig. 21. It is also clear from Fig. 23 that the virgin bitumen and the aged bitumen showed different fatigue crack lengths when subjected to the same loading conditions. The aged bitumen had a larger crack length compared to the virgin bitumen, which means the bitumen is subjected to more severe fatigue damage when undergoing oxidative ageing. This finding is consistent with that of the MD-based fatigue simulations discussed in Section 3.3.5.

## 4. Conclusions

In this study, the molecular origin of bitumen fatigue damage was investigated through molecular dynamics (MD) simulations. The molecular models were firstly constructed to represent virgin and aged PEN70/100 bitumen. The strain-controlled MD-based fatigue simulations with the COMPASS force field were then performed to study the nanostructure and damage behaviours of the virgin and aged bitumen under fatigue loading. The stress-strain response, potential energy, molecular structure, and nanovoid volumes were calculated based on simulation data. Furthermore, the rheometer measurements were conducted to characterise the fatigue damage of the bitumen by using a DSR-C model at the macroscale. The main findings from this study are as follows.



(a) A typical crack surface morphology.

(b) A circumferential crack.

Fig. 22. Schematic of fatigue crack in the bitumen sample under a DSR-based fatigue load.

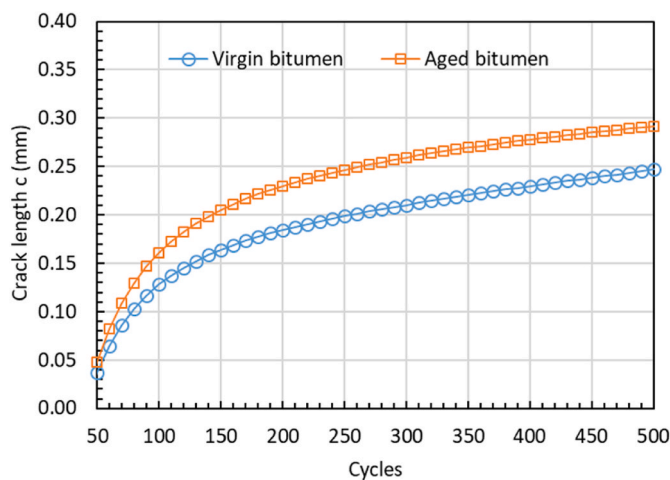


Fig. 23. Crack growth for the virgin and aged bitumen under a DSR-based fatigue load.

- (1) The molecular models of original and worn bitumen were developed based on their experimental data of elements, functional groups, molecular weights as well as saturate, aromatic, resin and asphaltene (SARA) fractions. The molecular dynamics (MD) fatigue simulations were then performed to investigate the nanostructures and damage behaviours of the original and worn bitumen by evaluating the stress-strain response, potential energy, molecular structure and nanovoid volumes during fatigue loading. The research results showed that the proposed computational approach based on MD simulations is capable of characterising the fatigue behaviours of the original and worn bitumen at the molecular scale.
- (2) Under tensile loading, the stress-strain curve of the aged bitumen exhibited a larger slope than that of the virgin bitumen, indicating a higher modulus. The developed MD model can be applied to investigate the viscoelastic behaviour and microscopic tensile failure (i.e. microcrack) of the bitumen by evaluating its stress-strain response and nanostructure change.

- (3) The stress relaxation of the bitumen at the molecular scale was found by MD simulations with a constant strain level, which indicate the viscoelastic characteristic of bitumen. The stress of the bitumen first decreased gradually and then remained stable with the increasing load cycles under strain-controlled fatigue loading.
- (4) When fatigue loading was applied, the bitumen molecules became unfolded and tend to align along the loading direction, which was indicated by the decreasing non-bond potential energy and the radius of gyration. The change in the molecular configuration helps the molecular chains move closer together and thus contributes to the reduction of the intermolecular interactions including the van der Waals and Coulombic energies.
- (5) Fatigue damage of bitumen at the molecular scale resulted from nanovoid formation and growth through molecular rearrangement and movement with the increasing fatigue load cycles. The aged bitumen exhibited higher nanovoid volume than the virgin bitumen, which is consistent with the findings from the DSR-based crack length under fatigue loading.

#### CRediT authorship contribution statement

**Yangming Gao:** Data curation, Investigation, Methodology, Writing – original draft. **Xueyan Liu:** Supervision, Writing – review & editing, Investigation, Resources. **Shisong Ren:** Data curation, Methodology. **Eli I. Assaf:** Methodology. **Pengfei Liu:** Funding acquisition, Writing – review & editing, Data curation. **Yuqing Zhang:** Writing – review & editing, Data curation.

#### Declaration of competing interest

The authors declare the following financial interests/personal relationships which may be considered as potential competing interests:

Yangming Gao reports financial support was provided by European Union. Pengfei Liu reports financial support was provided by German Research Foundation.

#### Data availability

Data will be made available on request.

## Acknowledgement

This work is part of a project that has received funding from the European Union's Horizon 2020 research and innovation programme under the Marie Skłodowska-Curie grant agreement No 101030767, and from the German Research Foundation (DFG) under Project No. LI 3613/3–1 with ID 528307766.

## References

- [1] Hajj R, Bhasin A. The search for a measure of fatigue cracking in asphalt binders—a review of different approaches. *Int J Pavement Eng* 2018;19(3):205–19.
- [2] Ghuzlan KA, Carpenter SH. Energy-derived, damage-based failure criterion for fatigue testing. *Transport Res Rec* 2000;1723(1):141–9.
- [3] Anderson DA, Le Hir YM, Marasteanu MO, Planche J-P, Martin D, Gauthier G. Evaluation of fatigue criteria for asphalt binders. *Transport Res Rec* 2001;1766(1): 48–56.
- [4] Bonnetti KS, Nam K, Bahia HU. Measuring and defining fatigue behavior of asphalt binders. *Transport Res Rec* 2002;1810(1):33–43.
- [5] Shen S, Carpenter SH. Application of the dissipated energy concept in fatigue endurance limit testing. *Transport Res Rec* 2005;1929(1):165–73.
- [6] Shen S, Airey GD, Carpenter SH, Huang H. A dissipated energy approach to fatigue evaluation. *Road Mater Pavement Des* 2006;7(1):47–69.
- [7] Shen S, Chiu H-M, Huang H. Characterization of fatigue and healing in asphalt binders. *J Mater Civ Eng* 2010;22(9):846–52.
- [8] Hintz C, Velasquez R, Johnson C, Bahia H. Modification and validation of linear amplitude sweep test for binder fatigue specification. *Transport Res Rec* 2011;2207 (1):99–106.
- [9] Hintz C, Bahia H. Simplification of linear amplitude sweep test and specification parameter. *Transport Res Rec* 2013;2370(1):10–6.
- [10] Underwood BS. A continuum damage model for asphalt cement and asphalt mastic fatigue. *Int J Fatig* 2016;82:387–401.
- [11] Hintz C, Bahia H. Understanding mechanisms leading to asphalt binder fatigue in the dynamic shear rheometer. *Road Mater Pavement Des* 2013;14(sup2):231–51.
- [12] Shan L, Tian S, He H, Ren N. Internal crack growth of asphalt binders during shear fatigue process. *Fuel* 2017;189:293–300.
- [13] Zhang Y, Gao Y. Predicting crack growth in viscoelastic bitumen under a rotational shear fatigue load. *Road Mater Pavement Des* 2019;1–20.
- [14] Gao Y, Li L, Zhang Y. Modeling crack propagation in bituminous binders under a rotational shear fatigue load using pseudo J-integral Paris' law. *Transportation Research Record*; 2020. 0361198119899151.
- [15] Gao Y, Li L, Zhang Y. Modelling crack initiation in bituminous binders under a rotational shear fatigue load. *Int J Fatig* 2020;139:105738.
- [16] Harvey J, Cebon D. Failure mechanisms in viscoelastic films. *J Mater Sci* 2003;38 (5):1021–32.
- [17] Poulikakos LD, Partl MN. Micro scale tensile behaviour of thin bitumen films. *Exp Mech* 2011;51(7):1171–83.
- [18] Poulikakos LD, Tiwari MK, Partl MN. Analysis of failure mechanism of bitumen films. *Fuel* 2013;106:437–47.
- [19] Sultana S, Bhasin A. Effect of chemical composition on rheology and mechanical properties of asphalt binder. *Construct Build Mater* 2014;72:293–300.
- [20] Hajj R, Ramm A, Bhasin A, Downer M. Real-time microscopic and rheometric observations of strain-driven cavitation instability underlying micro-crack formation in asphalt binders. *Int J Pavement Eng* 2019;1–13.
- [21] Office JE, Chen J, Dan H, Ding Y, Gao Y, Guo M, et al. New innovations in pavement materials and engineering: a review on pavement engineering research 2021. *J Traffic Transport Eng* 2021;8(6):815–999.
- [22] Du C, Liu P, Sun Y, Chen J, Liu Q, Oeser M. Characterizing asphalt mixtures with random aggregate gradations based on the three-dimensional locally homogeneous model. *Computer-Aided Civil and Infrastructure Engineering*; 2021.
- [23] Wollny I, Hartung F, Kaliske M, Liu P, Oeser M, Wang D, et al. Coupling of microstructural and macrostructural computational approaches for asphalt pavements under rolling tire load. *Comput Aided Civ Infrastruct Eng* 2020;35(11): 1178–93.
- [24] Rinaldini E, Schuetz P, Partl M, Tebaldi G, Poulikakos L. Investigating the blending of reclaimed asphalt with virgin materials using rheology, electron microscopy and computer tomography. *Compos B Eng* 2014;67:579–87.
- [25] Dong Z, Liu Z, Yang C, Gong X. Viscosity characterization of confined bitumen considering microaggregate-bitumen interactions. *Comput Aided Civ Infrastruct Eng* 2020;35(11):1261–75.
- [26] Gao Y, Zhang Y, Zhang C, Liu X, Jing R. Quantifying oxygen diffusion in bitumen films using molecular dynamics simulations. *Construct Build Mater* 2022;331: 127325.
- [27] Hou Y, Wang L, Wang D, Guo M, Liu P, Yu J. Characterization of bitumen micro-mechanical behaviors using AFM, phase dynamics theory and MD simulation. *Materials* 2017;10(2):208.
- [28] Hou Y, Wang L, Wang D, Qu X, Wu J. Using a molecular dynamics simulation to investigate asphalt nano-cracking under external loading conditions. *Appl Sci* 2017;7(8):770.
- [29] Du Z, Zhu X, Yuan Y. Molecular investigation on the adhesion and deformation behaviors of asphalt binder under nanoindentation. *Construct Build Mater* 2021; 295:123683.
- [30] Sun W, Wang H. Molecular dynamics simulation of nano-crack formation in asphalt binder with different SARA fractions. *Mol Simulat* 2022;1–12.
- [31] Lu Y, Wang L. Nanoscale modelling of mechanical properties of asphalt–aggregate interface under tensile loading. *Int J Pavement Eng* 2010;11(5):393–401.
- [32] Lu Y, Wang L. Nano-mechanics modelling of deformation and failure behaviours at asphalt–aggregate interfaces. *Int J Pavement Eng* 2011;12(4):311–23.
- [33] Xu G, Wang H. Molecular dynamics study of interfacial mechanical behavior between asphalt binder and mineral aggregate. *Construct Build Mater* 2016;121: 246–54.
- [34] Du Z, Zhu X, Li F, Zhou S, Dai Z. Failure of the asphalt–aggregate interface under tensile stress: insight from molecular dynamics. *J Mater Civ Eng* 2021;33(3): 04021008.
- [35] Chen P, Luo X, Gao Y, Zhang Y. Modelling percentages of cohesive and adhesive debonding in bitumen–aggregate interfaces using molecular dynamics approaches. *Appl Surf Sci* 2021;151318.
- [36] Li DD, Greenfield ML. Chemical compositions of improved model asphalt systems for molecular simulations. *Fuel* 2014;115:347–56.
- [37] Ren S, Liu X, Lin P, Erkens S, Xiao Y. Chemo-physical characterization and molecular dynamics simulation of long-term aging behaviors of bitumen. *Construct Build Mater* 2021;302:124437.
- [38] Petersen JC. A review of the fundamentals of asphalt oxidation: chemical, physicochemical, physical property, and durability relationships. *Transportation Research Circular*; 2009. E-C140.
- [39] Petersen JC, Glaser R. Asphalt oxidation mechanisms and the role of oxidation products on age hardening revisited. *Road Mater Pavement Des* 2011;12(4): 795–819.
- [40] Poulikakos LD, dos Santos S, Bueno M, Kuentzel S, Hugener M, Partl MN. Influence of short and long term aging on chemical, microstructural and macro-mechanical properties of recycled asphalt mixtures. *Construct Build Mater* 2014;51:414–23.
- [41] Allen MP, Tildesley DJ. *Computer simulation of liquids*. Oxford university press; 2017.
- [42] Sun H. COMPASS: an ab initio force-field optimized for condensed-phase applications overview with details on alkane and benzene compounds. *J Phys Chem B* 1998;102(38):7338–64.
- [43] Dong Z, Liu Z, Wang P, Gong X. Nanostructure characterization of asphalt–aggregate interface through molecular dynamics simulation and atomic force microscopy. *Fuel* 2017;189:155–63.
- [44] Gao Y, Zhang Y, Gu F, Xu T, Wang H. Impact of minerals and water on bitumen–mineral adhesion and debonding behaviours using molecular dynamics simulations. *Construct Build Mater* 2018;171:214–22.
- [45] Ren S, Liu X, Lin P, Erkens S, Gao Y. Chemical characterizations and molecular dynamics simulations on different rejuvenators for aged bitumen recycling. *Fuel* 2022;324:124550.
- [46] Weininger D. SMILES, a chemical language and information system. 1. Introduction to methodology and encoding rules. *J Chem Inf Comput Sci* 1988;28 (1):31–6.
- [47] Plimpton S. Fast parallel algorithms for short-range molecular dynamics. *J Comput Phys* 1995;117(1):1–19.
- [48] Venkatesan S, Basu S. Investigations into crazing in glassy amorphous polymers through molecular dynamics simulations. *J Mech Phys Solid* 2015;77:123–45.
- [49] Cormier J, Rickman J, Delph T. Stress calculation in atomistic simulations of perfect and imperfect solids. *J Appl Phys* 2001;89(1):99–104.
- [50] Chen Y. Local stress and heat flux in atomistic systems involving three-body forces. *J Chem Phys* 2006;124(5).
- [51] Cui T, Mukherjee S, Sudeep PM, Colas G, Najafi F, Tam J, et al. Fatigue of graphene. *Nat Mater* 2020;19(4):405–11.
- [52] Sahputra I, Echtermeyer A. Molecular dynamics simulations of strain-controlled fatigue behaviour of amorphous polyethylene. *J Polym Res* 2014;21(11):1–13.
- [53] Bowen L, Yong L, Jianzhong C, Li H, Xiaoyu Z. Fatigue performance of carbon fiber reinforced epoxy resin: a molecular simulation. *Polym Adv Technol* 2021;32(4): 1518–30.
- [54] Stukowski A. Visualization and analysis of atomistic simulation data with OVITO—the Open Visualization Tool. *Model Simulat Mater Sci Eng* 2009;18(1): 015012.
- [55] Gao Y, Zhang Y, Omairey EL, Al-Malaika S, Sheena H. Influence of anti-ageing compounds on rheological properties of bitumen. *J Clean Prod* 2021;318:128559.
- [56] Lesueur D. The colloidal structure of bitumen: consequences on the rheology and on the mechanisms of bitumen modification. *Adv Colloid Interface Sci* 2009;145 (1–2):42–82.
- [57] Xu G, Wang H. Molecular dynamics study of oxidative aging effect on asphalt binder properties. *Fuel* 2017;188:1–10.
- [58] Zhu X, Du Z, Ling H, Chen L, Wang Y. Effect of filler on thermodynamic and mechanical behaviour of asphalt mastic: a MD simulation study. *Int J Pavement Eng* 2020;21(10):1248–62.
- [59] Gao Y, Zhang Y, Yang Y, Zhang J, Gu F. Molecular dynamics investigation of interfacial adhesion between oxidised bitumen and mineral surfaces. *Appl Surf Sci* 2019;479:449–62.
- [60] Zhao G, Chen J, Lv Y, Zhang X, Huang L. Simulation of elastic and fatigue properties of epoxy/SiO<sub>2</sub> particle composites through molecular dynamics. *Comput Model Eng Sci* 2021;128(1):339–57.
- [61] Men Y, Rieger J, Lindner P, Enderle H-F, Lilge D, Kristen MO, et al. Structural changes and chain radius of gyration in cold-drawn polyethylene after annealing: small-and wide-angle X-ray scattering and small-angle neutron scattering studies 2005;109(35):16650–7.

- [62] Edelsbrunner H, Mücke EP. Three-dimensional alpha shapes. *ACM Trans Graph* 1994;13(1):43–72.
- [63] Hajj R, Mohanraj K, Bhasin A, Ramm A, Downer M. Micro-scale observations of fatigue damage mechanism in asphalt binder. In: *Advances in materials and pavement performance prediction II*. CRC Press; 2020. p. 449–53.
- [64] Gao Y. Multiscale modelling of bonding performance of bituminous materials. *Aston University*; 2020.